Endogenous cannabinoids are required for MC4R-mediated control of energy homeostasis

Yu Yong[a,1], Isin Cakir[b,1], Pauline Lining Pan[b], Jessica E. Biddinger[a], Rebecca J. Bluett[c], Ken Mackie[d], Nathan Bingham[e], Sachin Patel[a,c,2], and Masoud Ghamari-Langroudi[a,f,2]

[a]Department of Molecular Physiology and Biophysics, Vanderbilt University Medical Center, Nashville TN 37232; [b]Life Sciences Institute, University of Michigan, Ann Arbor, MI 48109; [c]Department of Psychiatry & Behavioral Sciences, Vanderbilt University Medical Center, Nashville TN 37232; [d]Department of Psychological & Brain Sciences, Indiana University, Bloomington, IN 47405; [e]Department of Pediatrics, Vanderbilt University Medical Center, Nashville TN 37232; and [f]Warren Center for Neuroscience Drug Discovery, Department of Pharmacology, Vanderbilt University, Nashville TN 37232

Edited by George Kunos, NIH, Bethesda, MD, and accepted by Editorial Board Member Susan G. Amara September 8, 2021 (received for review October 30, 2020)

Hypothalamic regulation of feeding and energy expenditure is a fundamental and evolutionarily conserved neurophysiological process critical for survival. Dysregulation of these processes, due to environmental or genetic causes, can lead to a variety of pathological conditions ranging from obesity to anorexia. Melanocortins and endogenous cannabinoids (eCBs) have been implicated in the regulation of feeding and energy homeostasis; however, the interaction between these signaling systems is poorly understood. Here, we show that the eCB 2-arachidonoylglycerol (2-AG) regulates the activity of melanocortin 4 receptor (MC4R) cells in the paraventricular nucleus of the hypothalamus (PVN^{MC4R}) via inhibition of afferent GABAergic drive. Furthermore, the tonicity of eCBs signaling is inversely proportional to energy state, and mice with impaired 2-AG synthesis within MC4R neurons weigh less, are hypophagic, exhibit increased energy expenditure, and are resistant to diet-induced obesity. These mice also exhibit MC4R agonist insensitivity, suggesting that the energy state–dependent, 2-AG-mediated suppression of GABA input modulates PVN^{MC4R} neuron activity to effectively respond to the MC4R natural ligands to regulate energy homeostasis. Furthermore, post-developmental disruption of PVN 2-AG synthesis results in hypophagia and death. These findings illustrate a functional interaction at the cellular level between two fundamental regulators of energy homeostasis, the melanocortin and eCB signaling pathways in the hypothalamic feeding circuitry.

endogenous cannabinoids | melanocortin 4 receptor | GABA neurotransmission | paraventricular nucleus of hypothalamus | energy homeostasis

In recent decades, the prevalence of disorders of energy homeostasis such as obesity has substantially increased (1–4). These disorders are commonly associated with increased rates of morbidity and mortality resulting in increased health care costs and decreased quality of life (5–7). A major underlying cause of obesity is overeating or eating in the absence of a negative energy balance due, in many instances, to a dysregulation of energy homeostasis. Despite recent advances, our knowledge of the physiology of feeding behavior has yielded few therapeutic tools to control disorders of energy homeostasis. Only recently, the Food and Drug Administration has approved the use of setmelanotide, a melanocortin 4 receptor (MC4R) agonist, for the treatment of severe childhood obesity caused by POMC mutations. Cannabinoid and endogenous cannabinoid (eCB) signaling have been heavily implicated in the regulation of food intake and energy expenditure (8, 9). However, how eCBs regulate hypothalamic feeding circuits in an energy state-dependent manner is not well understood.

Numerous studies support a crucial role for MC4R signaling in the regulation of energy balance (10–12). In particular, work by investigators during the past two decades underscores a unique role of the MC4R-expressing paraventricular hypothalamic (PVN) neurons and downstream neuronal pathways in regulating energy homeostasis (13–16). Pharmacological activation of MC4R, a Gsα-coupled receptor, results in suppression of food intake and insulin secretion and promotion of energy expenditure, cardiovascular activity, and lipid metabolism through the brainstem sympathomimetic pathways (17, 18). Mutations in the MC4R gene result in early onset severe hyperphagic obesity, decreased energy expenditure, hyperlipidemia, and a profile of metabolic syndrome in rodents and humans (10, 19). Due to its potent and unparalleled effect on energy homeostasis, MC4R has been a major target for development of therapeutic tools to treat obesity or cachexia (20–22). However, many attempts to activate MC4R signaling using orthosteric agonists have failed, mainly due to unwanted effects (23).

An alternate approach to directly targeting MC4R signaling, or core neurotransmitters and neuropeptides regulating these circuits, is targeting neuromodulatory systems that "fine-tune" activity within these circuits. Elucidating neuromodulatory mechanisms capable of altering the MC4R-expressing PVN (PVN^{MC4R}) neuron activity could reveal mechanisms to

Significance

Cannabis is well known to regulate food intake, and cannabinoids increase the value of caloric and non-caloric rewards, while also regulating homeostatic feeding. Here, we show that tonic endogenous cannabinoid signaling regulates the melanocortin 4 receptor (MC4R) expressing paraventricular hypothalamic neurons through modulation of their presynaptic inhibitory inputs in an energy state–dependent manner. Specifically, this tonic 2-AG signal is maximal during fasting and collapses in satiation. Impairing 2-AG synthetic capacity from MC4R neurons reduces body weight and confers resistance to diet-induced obesity via increased energy expenditure and reduced food intake. This mode of regulation of MC4R neurons could offer a new therapeutic avenue to modulate food intake and energy metabolism.

Author contributions: I.C., N.B., and M.G.-L. designed research; Y.Y., I.C., P.L.P., J.E.B., R.J.B., and M.G.-L. performed research; K.M., N.B., S.P., and M.G.-L. contributed new reagents/analytic tools; I.C. and M.G.-L. analyzed data; and I.C. and M.G.-L. wrote the paper.

The authors declare no competing interest.

This article is a PNAS Direct Submission. G.K. is a guest editor invited by the Editorial Board.

[1]Y.Y. and I.C. contributed equally to this work.

[2]To whom correspondence may be addressed. Email: masoud.ghamari-langroudi@vanderbilt.edu or sachin.patel@vumc.org.

This article contains supporting information online at http://www.pnas.org/lookup/suppl/doi:10.1073/pnas.2015990118/-/DCSupplemental.

Published October 15, 2021.

regulate food intake, energy expenditure, and opportunities for therapeutic intervention for disorders of food intake such as obesity. One such neuromodulatory system is the eCB system (8, 9). eCBs are arachidonate-based neurotransmitters produced and released by the postsynaptic cell. Subsequently, eCBs diffuse and bind to presynaptic Giα-coupled cannabinoid receptors, mainly the CB1 receptor (CB1R), to inhibit presynaptic neurotransmitter release (24). The two main eCBs are anandamide (N-arachidonoylethanolamide, AEA) and 2-arachidonoylglycerol (2-AG), which are produced throughout the mammalian central and peripheral nervous system. 2-AG is synthesized by diacylglycerol lipase alpha (DAGLα) in postsynaptic neurons and is degraded by monoacylglycerol lipase (MAGL) localized to presynaptic axon terminals (25). The capacity of cannabinoids to regulate feeding behavior has long been known (26, 27). However, the cellular, synaptic, and circuit-level mechanisms by which eCBs regulate food intake and energy homeostasis are incompletely understood.

Here, we use a variety of in vivo and ex vivo approaches combining genetic and pharmacological tools to elucidate the mechanism by which 2-AG signaling regulates food intake and energy expenditure. We demonstrate that 2-AG regulates the activity of lateral parabrachial nucleus (LPBN)–projecting PVN^{MC4R} neurons via inhibition of presynaptic GABA release onto this subset of PVN^{MC4R} neurons. We further show that mice with impaired 2-AG synthesis in PVN^{MC4R} neurons are hypophagic, weigh less, and are resistant to obesogenic and diabeteogenic challenges. These data provide insights into the mechanisms regulating PVN^{MC4R} neuron activity and the mechanisms by which 2-AG signaling affects feeding and energy homeostasis.

Results

Food Deprivation Increases the Activity of PVN^{MC4R} Neurons via Suppression of GABA Release. Given the central role of PVN^{MC4R} neurons in controlling energy balance, we first investigated how their activity is regulated by energy state. Utilizing cell-attached recordings in acute brain slices from MC4R-GFP mice we found that 16 h of fasting significantly increased action potential (AP) firing frequency of PVN^{MC4R} neurons relative to ad libitum controls (Fig. 1*A*). The c-fos expression also significantly increased in the ventral subregions of PVN^{MC4R} where most recordings were obtained (*SI Appendix*, Fig. S1). GABAergic inputs from the arcuate nucleus of the hypothalamus are a strong regulator of PVN neuron activity (28). We thus hypothesized that this fasting-induced increase in AP frequency could be due to reduced GABAergic tone onto PVN^{MC4R} neurons. Using whole-cell patch clamp, we found that fasting significantly reduced miniature Inhibitory Postsynaptic Current (mIPSC) frequency recorded from PVN^{MC4R} neurons (Fig. 1*B*). Numerous studies have suggested that a subset of PVN neurons that project to the LPBN play a role in regulating feeding, thermogenesis, and body weight (29, 30). Thus, we next specifically examined the effect of fasting on the PVN^{MC4R}→LPBN neurons. We performed bilateral LPBN injections of an RFP-retrograde viral vector in MC4R-GFP mice and recorded from double-labeled PVN neurons. The mean AP firing frequency of PVN^{MC4R}→LPBN neurons increased more than twofold after 16 h of fasting compared to ad libitum–fed mice (Fig. 1*C*). Moreover, 2-h refeeding after an overnight fast significantly suppressed AP firing compared to fasted mice, although not completely to the levels observed in ad libitum–fed mice (Fig. 1*C*). These results suggest that the activity of the PVN^{MC4R}→LPBN neurons inversely correlates with energy state.

Endocannabinoids Mediate Food Deprivation–Induced Suppression of GABA Input to PVN^{MC4R} Neurons. Cannabinoid and eCB signaling have been heavily implicated in the regulation of food intake, energy homeostasis, and obesity (8, 9). Furthermore, recent studies support the model that hypothalamic eCB signaling fluctuates as a function of energy stores in mice (31). Using mass spectrometry to quantify 2-AG in tissue samples, we found that overnight fasting increased 2-AG levels compared to the ad libitum–fed condition in the PVN but not amygdala (Fig. 1*D*) (32). Additionally, N-oleoyl ethanolamine (OEA) and N-palmitoyl ethanolamine (PEA) but not AEA were significantly increased by fasting in PVN but not in amygdala (*SI Appendix*, Fig. S2). Given that 2-AG is a prominent regulator of GABAergic transmission in the PVN (33), we hypothesized that the tonicity of 2-AG—CB1R signaling is enhanced after fasting to suppress GABAergic afferent input converging onto these neurons. We tested this hypothesis by analyzing the effects of SR141716, a potent CB1R blocker, on the frequency of mIPSCs in PVN^{MC4R}. Brain slices from mice that were 16 h fasted or ad libitum fed were preincubated for 1 h with SR141716 or vehicle before performing recordings. SR141716 significantly increased the frequency of mIPSCs in PVN^{MC4R} neurons from fasted but not ad libitum–fed mice (Fig. 1*E*). Furthermore, the mean frequency of mIPSCs from SR141716-treated, fasted mice was not different from that of the vehicle or of the SR141716-treated fed mice (Fig. 1*E*). Given that 2-AG levels were increased in the PVN after fasting, we hypothesized that 2-AG was responsible for this CB1R-mediated suppression of GABA release onto PVN^{MC4R} neurons after fasting. To test this, we first compared the frequency of mIPSCs in slices from fed mice that were pretreated with vehicle or an inhibitor of 2-AG degradation (JZL184). As expected, enhancing 2-AG signaling by preventing its degradation resulted in suppression of PVN^{MC4R} neuron mIPSCs in slices from fed mice. We then hypothesized that the blockade of 2-AG synthesis would increase mIPSC frequency in slices from fasted mice, similar to the effects of SR141716. Indeed, pretreatment with DO34, an inhibitor of the 2-AG synthesizing enzyme DAGL, increased the mIPSC frequency in PVN^{MC4R} neurons in overnight-fasted mice. There was no difference between mIPSC frequency from JZL184-treated, fed mice and DO34-treated, fasted mice (Fig. 1*F*). We further examined whether 2-AG-mediated suppression of mIPSCs during fasting would also affect the frequency of somatic APs. Similar to Fig. 1*F*, we measured the effect of JZL184 pretreatment on AP firing frequency in slices from fed mice. JZL184 pretreatment significantly increased AP firing frequency, compared to vehicle pretreatment, in slices from fed mice. Furthermore, DO34 pretreatment of slices from fasted mice significantly suppressed the AP frequency of PVN^{MC4R} neurons (Fig. 1*G*). These findings suggest that 2-AG tonically suppresses presynaptic GABA release leading to increases in activity of PVN^{MC4R} neurons in the fasted state. Consistent with these findings, results from fluorescence in situ hybridization (FISH, *SI Appendix*, Fig. S3) and immunohistochemistry (IHC, *SI Appendix*, Fig. S4) assays indicate that the levels of DAGLα transcripts and protein, respectively, increase in PVN^{MC4R} neurons after 24 h fasting.

Suppression of Endocannabinoid Synthesis Decreases Food Intake after Fasting. Our data indicate that the activity of PVN^{MC4R} neurons is highest during fasting, suggesting that their activity could facilitate feeding and/or signal energy deficiency. Thus, decreasing the AP firing of the PVN^{MC4R} neurons by suppressing 2-AG synthesis with DO34 (i.e., maintaining high GABA transmission) should reduce food intake in the fasted state. Indeed, in 24 h–fasted mice, DO34 (injected intraperitoneally; ip) significantly suppressed cumulative food intake from 12 to

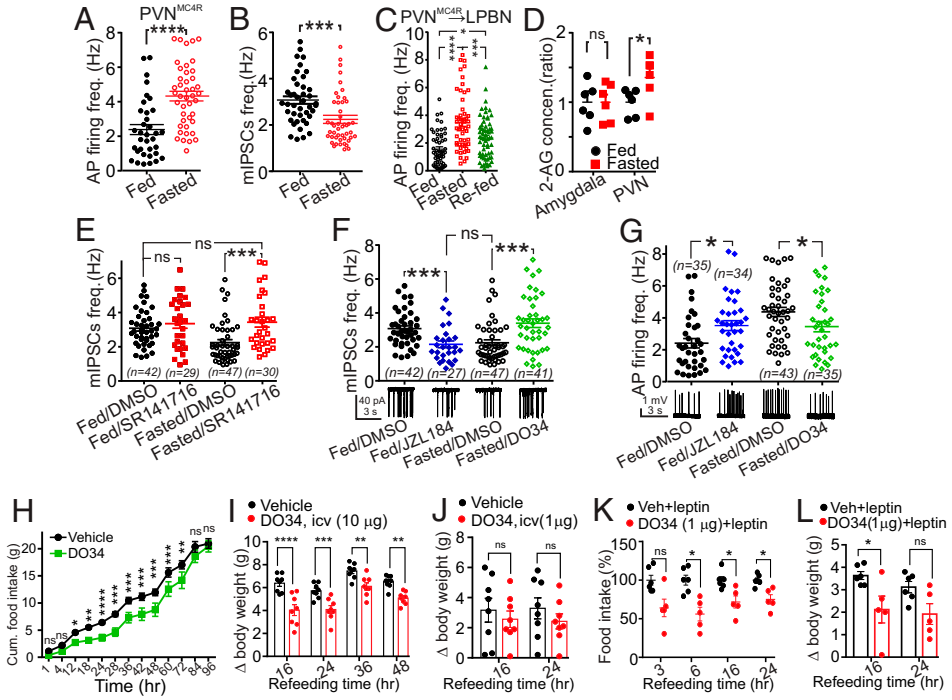

Fig. 1. Fasting increases the tonicity of 2-AG signaling in LPBN-projecting PVN^{MC4R} neurons to promote feeding. (*A*) Scatter plots of the AP firing frequency of PVN^{MC4R} cells recorded from acute hypothalamic slices from MC4R-GFP mice in ad libitum feeding (n = 35) and after an overnight fast (n = 43, unpaired t test). Four to eight mice were used to record AP activity for each experimental subgroup presented. (*B*) Scatter plots of the mIPSC frequency of PVN^{MC4R} cells in ad libitum feeding (n = 42) and after an overnight fast (n = 47, unpaired t test). (*C*) Scatter plots of the AP firing frequency of PVN^{MC4R}→LPBN neurons recorded from mice that were ad libitum fed (n = 55, six mice), overnight fasted (n = 55, eight mice), and overnight fasted with 2-h refeeding (n = 62, four mice, one-way ANOVA). (*D*) Fasted over fed ratios of the mass spectrometry quantification of 2-AG concentrations in PVN (n = 6) and amygdala (n = 6, unpaired t test) from 1-mm-thick brain punches. (*E*) Scatter plots of the mIPSC frequency recorded from PVN^{MC4R} cells from ad libitum–fed mice pretreated with CB1 receptor antagonist (SR141716, n = 29) or with vehicle (DMSO, n = 42) and overnight-fasted mice pretreated with CB1 receptor antagonist (n = 30) or with vehicle. Five to 10 mice were used to record mIPSC frequency for each experimental subgroup presented (n = 47, one-way ANOVA, Tukey's multiple comparisons test). (*F*) Scatter plots of the mIPSC frequency recorded from PVN^{MC4R} cells from ad libitum–fed mice pretreated with MAGL inhibitor (JZL184, n = 27) or with vehicle (n = 42) and overnight-fasted mice pretreated with DAGL inhibitor (DO34, n = 41) or with vehicle (n = 47, one-way ANOVA, Tukey's multiple comparisons test). (*G*) Scatter plots of the AP firing frequency recorded from PVN^{MC4R} cells from ad libitum–fed mice pretreated with MAGL inhibitor (JZL184, n = 34) or with vehicle (n = 35, unpaired t test) and overnight-fasted mice pretreated with DAGL inhibitor (DO34, n = 35) or with vehicle (n = 43, unpaired t test). (*H*) Cumulative food intake of 24-h–fasted wild-type mice injected ip with D034 (50 mg/kg, n = 4 cages, 19 mice), an inhibitor of DAGLα, or vehicle (n = 4 cages, 20 mice) just before the dark onset (Sidak's multiple comparisons test, two-way ANOVA). (*I*) Body weight change of 24 h–fasted wild-type mice treated with icv vehicle (n = 8) or DO34 (10μg/mouse, n = 8). Icv injection of DO34 (10 μg) also led to suppression weight gain in fasted mice. (*J*) Body weight change of 24 h–fasted wild-type mice treated with icv vehicle (n = 8) or DO34 (1 μg/mouse, n = 8). Icv injection of DO34 (1 μg) failed to alter weight gain in fasted mice. (*K*, *L*) Food intake (*K*) and weight change (*L*) of 24 h–fasted wild-type mice treated with icv vehicle or DO34 (1μg/mouse) and cotreated with ip vehicle or leptin (Sidak's multiple comparisons test, two-way ANOVA for *I* through *L*). Data are presented as mean ± SEM. ns indicates $P > 0.05$, * indicates $P < 0.05$, ** indicates $P < 0.01$, *** indicates $P < 0.001$, and **** indicates $P < 0.0001$.

72 h of refeeding (Fig. 1*H*). Analysis of hourly food intake indicated that DO34 significantly suppressed refeeding up to 28 h compared to vehicle (*SI Appendix*, Fig. S5*A*). Furthermore, 84 h after refeeding, DO34-treated mice significantly increased food intake, presumably to compensate for their energy deficit (*SI Appendix*, Fig. S5*A*). Because DAGL expression is not restricted to the CNS, we next infused DO34 centrally. Intracerebroventricular (icv) injection of DO34 (10 μg) also led to the suppression of food intake (*SI Appendix*, Fig. S5*B*) and weight gain in fasted mice (Fig. 1*I*). The suppressive effect of DO34 on weight gain lasted longer than its effect on food intake, suggesting that DO34 also promoted energy expenditure. Peripheral CB1R antagonism reverses leptin resistance and induces weight loss (34). Because leptin acts upstream of the PVN^{MC4R} neurons, we tested whether the anorectic action of leptin would be augmented when 2-AG signaling was centrally blocked. To this end, we first identified a lower icv dose of DO34 (1 μg) that did not alter food intake or body weight (Fig. 1*J* and *SI Appendix*, Fig. S5*C*). However, when we coadministered leptin with this dose of DO34, the anorectic effect of leptin was potentiated (Fig. 1 *K* and *L*), suggesting a synergistic effect between the central action of 2-AG and leptin.

Genetic Deletion of 2-AG Synthesis from MC4R Neurons Reduces Food Intake and Body Weight. Since both systemic and central suppression of 2-AG signaling reduce food intake, we hypothesized that mice with an MC4R neuron-specific deficit in 2-AG synthesis would also have lower food intake and body weight. To test this hypothesis, we generated mice with DAGLα deleted specifically from the MC4R neurons (MC4R$^{\Delta DAGL\alpha}$) by crossing floxed-DAGLα mice with the MC4R-Cre mice (16). The body weight of MC4R$^{\Delta DAGL\alpha}$ mice was significantly lower than MC4R-Cre controls starting at 17 wk of age. MC4R$^{\Delta DAGL\alpha}$ mice weighed ∼10% less at 20 wk and 14% less at 30 wk of age than the Cre control mice (Fig. 2*A*). MC4R$^{\Delta DAGL\alpha}$ mice also consumed less chow per day compared to MC4R-Cre control mice (Fig. 2*B*).

MC4R$^{\Delta DAGL\alpha}$ Mice Resist Diet-Induced Obesity. Since MC4R$^{\Delta DAGL\alpha}$ mice eat less than their control counterparts, we hypothesized that they would be resistant to weight gain under a calorie enriched diet. We thus placed adult male mice on highfat diet (HFD) (60% calories from fat) for 8 wk and monitored their body weight and food intake. With normal chow, the MC4R$^{\Delta DAGL\alpha}$ mice weighed about 5 gm less than their Cre controls. After just 1 wk of ad libitum HFD access, MC4R$^{\Delta DAGL\alpha}$ mice weighed about 6 grams less than MC4R-Cre mice, and after 8 wk, the MC4R$^{\Delta DAGL\alpha}$ mice weighed about 14 gm (26%) less than their MC4R-Cre counterparts (Fig. 2*C*).

Male MC4R$^{\Delta DAGL\alpha}$ mice consumed less regular chow and HFD (Fig. 2*D*). When food intake was converted to calorie intake, MC4R$^{\Delta DAGL\alpha}$ mice consumed less on both regular

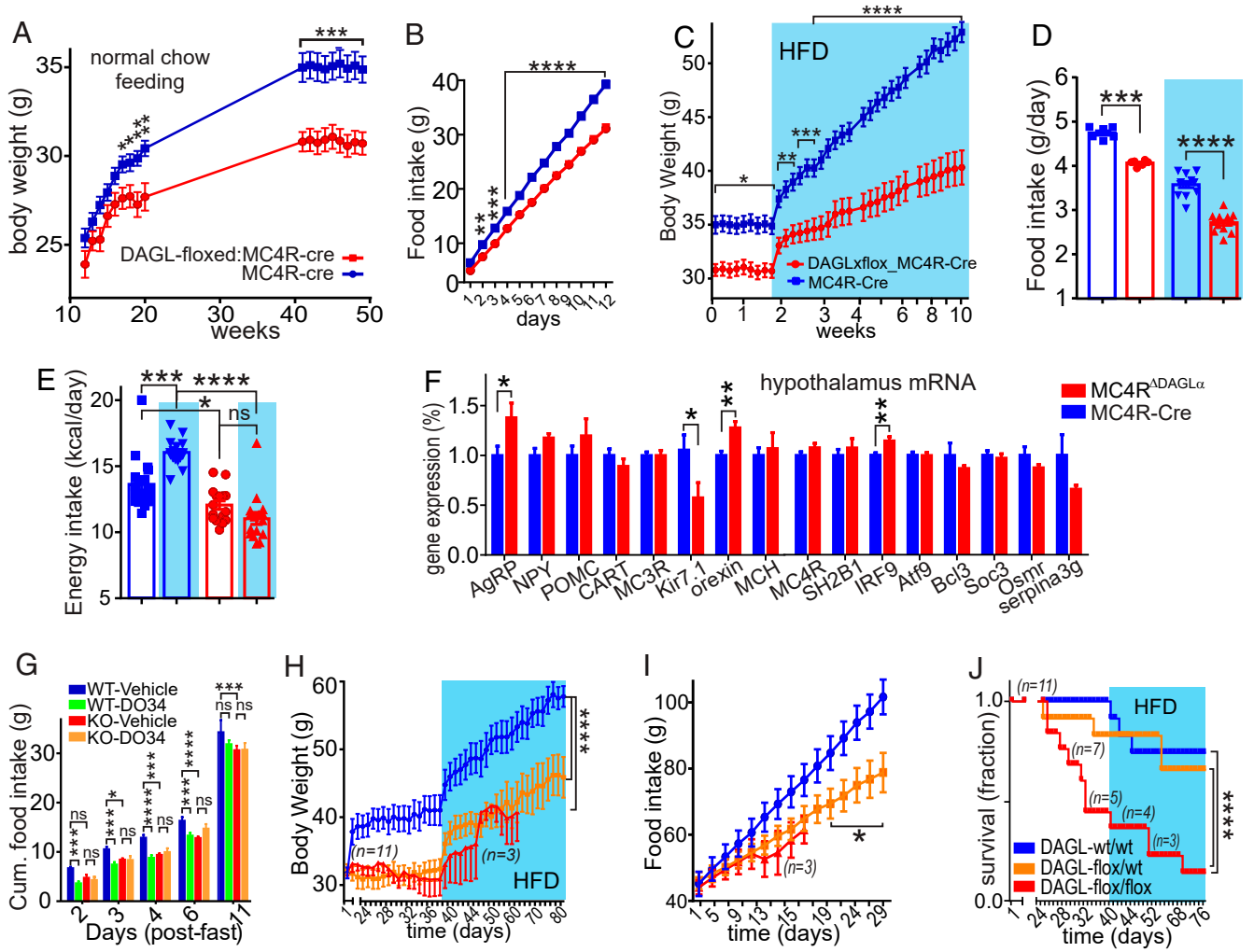

Fig. 2. 2-AG signaling in hypothalamic MC4R neurons is required for regulation of body weight and homeostatic feeding. (*A*) Graphs indicate the body weight of male MC4R$^{\Delta DAGL\alpha}$ mice (DAGL$\alpha^{loxP/loxP}$:MC4R-Cre, n = 24) compared with their control (DAGL$\alpha^{+/+}$:MC4R-Cre, n = 23, two-way ANOVA, Sidak's multiple-comparisons test). (*B*) Graphs indicate the cumulative normal chow food intake consumed in 2 wk by 24-wk-old male MC4R$^{\Delta DAGL\alpha}$ mice (n = 12) and MC4R-Cre control mice (n = 12). This difference reached significant after 2 d of measurement of food intake (n = 12 each group, two-way ANOVA, Sidak's multiple-comparisons test). (*C*) Graphs indicate body weight of male 24-wk-old MC4R$^{\Delta DAGL\alpha}$ mice (n = 16) and MC4R-Cre (n = 19) mice on ad libitum normal chow and hight-fat diet (blue shade, two-way ANOVA, Sidak's multiple-comparisons test). (*D*) Bar graphs indicate the mass of food taken (fed with feeders) by 24-wk-old male MC4R$^{\Delta DAGL\alpha}$ mice (n = 16) and MC4R-Cre (n = 18) mice averaged over 1 wk during normal chow feeding and 1 wk of HFD feeding (blue shade, one-way ANOVA, Tukey's multiple-comparisons test). (*E*) Bar graphs indicate the calories taken by male MC4R$^{\Delta DAGL\alpha}$ mice (n = 16) and MC4R-Cre (n = 18) mice averaged over 1 wk during normal chow feeding and 1 wk of HFD feeding (blue shade, one-way ANOVA, Tukey's multiple-comparisons test). (*F*) Bar graphs indicate the expression of certain genes normalized to the TBP gene in hypothalamic explants by using qPCR from MC4R$^{\Delta DAGL\alpha}$ (n = 9) and MC4R-Cre mice (n = 8) after 12 wk of HFD feeding (unpaired t test). (*G*) Bar graphs indicate cumulative ad libitum food intake of 34-wk-old male MC4R$^{\Delta DAGL\alpha}$ (n = 24) and MC4R-Cre (n = 25) mice fasted for 24 h and then injected with either DO34 or vehicle ip just before the beginning of the dark cycle, and food intake was measured for the subsequent 11 d (two-way ANOVA, Tukey's multiple-comparisons test). (*H–J*) Cre-expressing viral vector was injected into bilateral PVN in DAGL$\alpha^{flox/flox}$,(n = 11) DAGL$\alpha^{flox/wt}$ (n = 12) and DAGL$\alpha^{wt/wt}$ (n = 10) adult male mice and body weight (*H*), food intake (*I*), and survival rate (*J*) were measured starting from 3 wk after viral injections feeding on normal chow diet and HFD for additional 6 wk (blue shade). A total 11 DAGL$\alpha^{flox/flox}$, mice were injected with Cre containing viral vector. This group was excluded from analysis after 2 wk of feeding HFD when n value reached less than 3 (ordinary one-way ANOVA). Data are presented as mean ± SEM. ns indicates $P > 0.05$, * indicates $P < 0.05$, ** indicates $P < 0.01$, *** indicates $P < 0.001$, and **** indicates $P < 0.0001$.

chow and HFD than MC4R-Cre controls. Notably, unlike the controls, MC4R$^{\Delta DAGL\alpha}$ mice failed to display the HFD-induced increase in calorie intake (Fig. 2*E*) (35). These results suggest a perturbation in the hypothalamic regulation of body weight in MC4R$^{\Delta DAGL\alpha}$ mice. We thus used qPCR to analyze hypothalamic expression of genes that are involved in energy homeostasis. Normalized values indicate significant increases in expression of AgRP and orexin and a decrease in the expression of Kir7.1 in MC4R$^{\Delta DAGL\alpha}$ mice compared to Cre counterparts (Fig. 2*F*), consistent with a negative energy balance in the hypothalamic circuits of MC4R$^{\Delta DAGL\alpha}$ mice.

MC4R is expressed in the periphery, most notably in the enteroendocrine L cells (36). To rule out the potential involvement of the peripheral DAGLα downstream to MC4R signaling in energy balance parameters, we reconstituted the endogenous MC4R expression specifically in the epithelial cells of the intestine. To this end, we crossed the Villin-Cre mice to MC4R-TB mice (13, 37), in which endogenous expression of MC4R can be rescued by Cre-mediated deletion of a stop cassette, to generate MC4R^{Vil} mice. The MC4R agonist α-MSH reduced the short-circuit current (I_{SC}) (36) when applied to the intestines from wild-type and MC4R^{Vil} mice but not the MC4R^{TB} mice,

suggesting the successful rescue of the MC4R expression in the $MC4R^{Vil}$ mice (*SI Appendix*, Fig. S6*A*). Re-expression of MC4R specifically in the gut ($MC4R^{Vil}$) in the MC4R knockout background did not rescue the obesity phenotype of MC4R-TB mice in either sex (*SI Appendix*, Fig. S6 *B* and *C*). Furthermore, when fed HFD, the body weights of the $MC4R^{Vil}$ mice were not different from the MC4R-TB mice, and both groups gained significantly more weight than the wild-type counterparts (*SI Appendix*, Fig. S6*D*). Notably, the MC4R agonist LY did not alter the body weight of the MC4R-TB or $MC4R^{Vil}$ mice (*SI Appendix*, Fig. S6*E*). These results collectively suggest that peripheral MC4R expression does not significantly contribute to the regulation of energy balance.

Hypophagic Effects of DAGL Inhibition and MC4R Agonists Are Absent in $MC4R^{\Delta DAGL\alpha}$ Mice. In order to confirm that the food intake–suppressing effect of DO34 was mediated via similar circuits as that observed in $MC4R^{\Delta DAGL\alpha}$ mice, we tested the hypothesis that DO34 would fail to suppress food intake in fasted $MC4R^{\Delta DAGL\alpha}$ mice. Twenty four-hour-fasted $MC4R^{\Delta DAGL\alpha}$ and MC4R-Cre mice were injected with either DO34 or vehicle, and food intake was measured for the subsequent 11 d. Analysis of cumulative food intake during the refeeding period reveals several important findings. First, vehicle-injected $MC4R^{\Delta DAGL\alpha}$ mice consumed less food than the vehicle-injected MC4R-Cre mice (Fig. 2*G*), extending our previous findings of decreased intake without fasting (Fig. 2*B*). Second, the DO34-treated MC4R-Cre mice consumed significantly less food than the vehicle-treated MC4R-Cre mice at all time points measured (Fig. 2*G*), as observed previously in wild-type mice (Fig. 1*H*). Importantly, the DO34-treated $MC4R^{\Delta DAGL\alpha}$ mice consumed a similar amount of food to vehicle-treated $MC4R^{\Delta DAGL\alpha}$ mice at all time points (Fig. 2*G*). The occlusion of DO34-induced anorexia in $MC4R^{\Delta DAGL\alpha}$ mice indicates that the anorexigenic effect of DO34 depends on DAGLα activity within MC4R cells (Fig. 2*G*). We further examined the functionality of the MC4R neurons in $MC4R^{\Delta DAGL\alpha}$ mice by testing the anorexigenic effects of the MC4R selective agonist, LY2112688, on postfast refeeding kinetics. Male 12-wk-old mice fed on normal chow were fasted for 24 h and injected ip with LY2112688 1 h before the dark cycle. LY2112688 failed to suppress food intake beyond the initial 2-h time point in $MC4R^{\Delta DAGL\alpha}$ mice compared to Cre controls (*SI Appendix*, Fig. S7). These findings suggest that the ability of MC4R activation to suppress food intake requires 2-AG synthesis from MC4R cells.

PVN-Restricted Deletion of DAGLα Results in Decreased Body Weight, Food Intake, and Survival. Given that MC4R is expressed widely in the brain and Cre is also constitutively expressed throughout development in MC4R-Cre mice, DAGLα is deleted from all MC4R neurons from very early developmental age in $MC4R^{\Delta DAGL\alpha}$ mice (38). To exclude the possibility of developmental effects, we investigated the impact of postdevelopmental DAGLα deletion from the PVN on the regulation of energy homeostasis. A Cre-expressing viral vector (AAV9-Cre) was injected bilaterally into the PVN of $DAGL\alpha^{flox/flox}$, $DAGL\alpha^{flox/wt}$, and $DAGL\alpha^{wt/wt}$ adult male mice. The body weights of both $DAGL\alpha^{flox/flox}$ and $DAGL\alpha^{flox/wt}$ mice with ad libitum access to normal chow was significantly lower than $DAGL\alpha^{wt/wt}$ counterparts at 3 wk post injection (Fig. 2*H*). The body weight of the $DAGL\alpha^{flox/flox}$ group was not different from $DAGL\alpha^{flox/wt}$ mice. This trend continued during high-fat diet feeding. After 6 wk of HFD, the body weights of $DAGL\alpha^{flox/wt}$ mice were significantly lower than $DAGL\alpha^{wt/wt}$ counterparts (Fig. 2*H*). The cumulative food intake was also significantly lower in $DAGL\alpha^{flox/flox}$ and $DAGL\alpha^{flox/wt}$ mice than $DAGL\alpha^{wt/wt}$ counterparts (Fig. 2*I*). Interestingly, $DAGL\alpha^{flox/flox}$ mice had a significantly lower survival rate (45%) compared to both $DAGL\alpha^{flox/wt}$ (85%) and $DAGL\alpha^{wt/wt}$ (90%) counterparts measured at 4 wk post injections; given the reduced group size, $DAGL\alpha^{flox/flox}$ were excluded from analysis after week 6 of HFD (Fig. 2 *H–J*). Our observation suggests that hypophagia and weight loss preceded death in PVN-Cre-$DAGL\alpha^{flox/flox}$ mice. These findings demonstrate that postdevelopmental deletion of PVN DAGLα results in decreased body weight, food intake, and survival rate in a gene dosage-dependent manner, suggesting that both PVN *DAGLα* alleles are required for normal energy homeostasis. Furthermore, the hypophagia and dietinduced obesity (DIO)-resistance of $MC4R^{\Delta DAGL\alpha}$ mice may be mediated via actions within the PVN^{MC4R} neurons. Postdevelopmental deletion of DAGLα is potentially more lethal compared to the $MC4R^{\Delta DAGL\alpha}$, because here, DAGLα was deleted from all cells in the PVN, not only PVN^{MC4R}. Alternatively, it's possible that embryonic deletion of DAGLα results in developmental compensation to preserve the function of this critical feeding circuit, as when the upstream AgRP neurons are ablated neonatally (39, 40).

$MC4R^{\Delta DAGL\alpha}$ Mice Are Resistant to Metabolic Syndrome and to Obesogenic and Diabetogenic Challenges. We hypothesized that the decreased body weight of $MC4R^{\Delta DAGL\alpha}$ mice could be due to decreased adiposity. We thus analyzed the body composition of 50-wk-old male $MC4R^{\Delta DAGL\alpha}$ mice and MC4R-Cre mice after 12 wk of HFD feeding. $MC4R^{\Delta DAGL\alpha}$ mice had similar lean mass but lower fat mass compared to MC4R-Cre mice. Furthermore, $MC4R^{\Delta DAGL\alpha}$ mice had a higher percentage of lean mass and lower percentage of fat compared to MC4R-Cre mice (Fig. 3 *A–C*). Consistent with these findings, the serum levels of leptin were also lower in $MC4R^{\Delta DAGL\alpha}$ mice than in MC4R-Cre counterparts (Fig. 3*D*). These results indicate decreased adiposity and altered distribution of body mass in $MC4R^{\Delta DAGL\alpha}$ mice compared to MC4R-Cre controls.

To understand the molecular mechanisms underlying the resistance of $MC4R^{\Delta DAGL\alpha}$ mice to obesogenic and diabetogenic challenges, we performed gene expression analysis using qRT-PCR to examine the messenger RNA (mRNA) expression of genes that regulate lipid and glucose homeostasis in epididymal and inguinal white adipose tissue (eWAT and iWAT, respectively). In the eWAT, there were significant increases in the expression of Fasn, pparα, scd1, and Acaca and decreases in IL10 and TNFα in $MC4R^{\Delta DAGL\alpha}$ mice compared to Cre counterparts (Fig. 3*E*). In iWAT, there were significant increases in the expression of PGC1α and scd1 (Fig. 3*F*). These results collectively suggest increased fatty acid synthesis, adipocyte "beiging," and increased lipogenesis indicating an anabolic state in $MC4R^{\Delta DAGL\alpha}$ mice. Liver sections stained with hematoxylin and eosin indicate that $MC4R^{\Delta DAGL\alpha}$ mice are resistant to fatty liver demonstrated by significant decreases in fat vacuole size (Fig. 3 *G–I*). To understand the molecular mechanisms underlying the resistance of $MC4R^{\Delta DAGL\alpha}$ mice to fatty liver, we investigated expression of genes which play a role in metabolism and glucose homeostasis. Analysis of liver tissue indicates a significant increase in the expression of PCK1 and significant decreases of pparγ, Lp1, cd36, and FGF21 in $MC4R^{\Delta DAGL\alpha}$ mice (Fig. 3*J*), suggesting a profile of improved liver function, insulin sensitivity, and reduced inflammation under HFD feeding in $MC4R^{\Delta DAGL\alpha}$ mice compared to Cre animals.

$MC4R^{\Delta DAGL\alpha}$ Mice Exhibit Improved Glucose Tolerance and Insulin Sensitivity. Consistent with decreased adiposity and lower hepatic steatosis, fasting blood glucose and serum insulin levels were lower in $MC4R^{\Delta DAGL\alpha}$ mice than Cre mice (Fig. 3 *K* and *L*). These findings collectively represent a profile of improved metabolic syndrome and glucose homeostasis in the

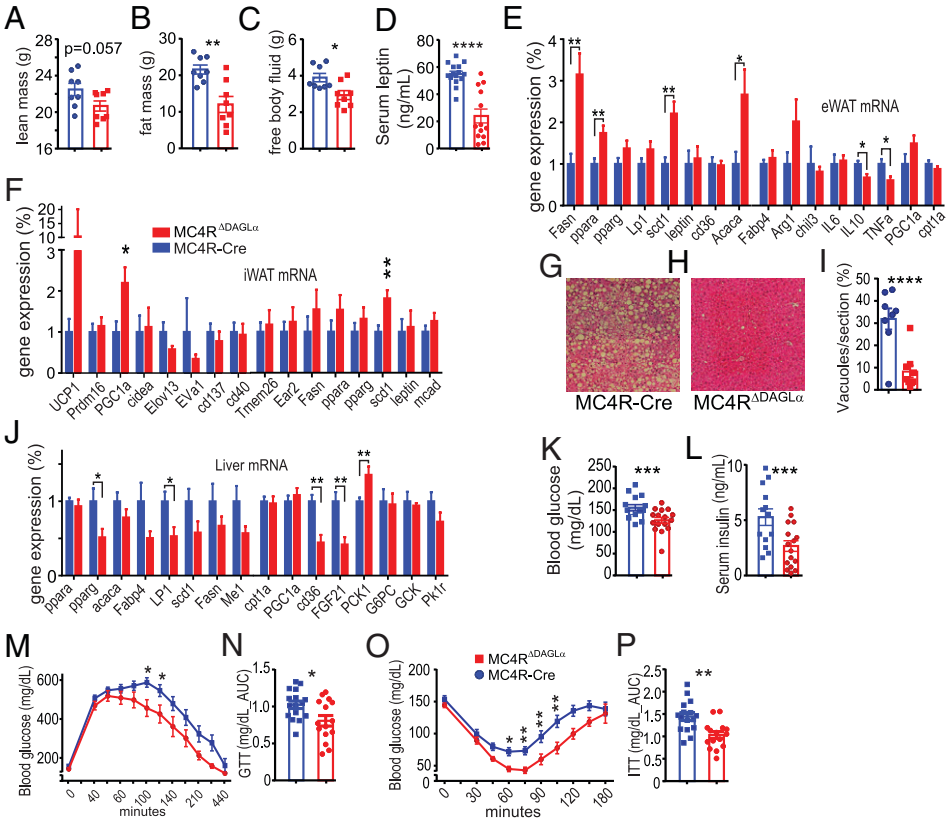

Fig. 3. Deletion of 2-AG synthesis in MC4R neurons protects against obesogenic and diabetegenic challenges. (*A–C*) Bar graphs indicate parameters of body composition of 50-wk-old male MC4R$^{\Delta DAGL\alpha}$ (n = 8) and MC4R-Cre (n = 8) mice after 12 wk of feeding ad libitum on HFD by using TD-NMR systems, (*A*) the absolute amount lean mass, (*B*) the absolute amount fat mass, and (*C*) the absolute mass of free body fluid (unpaired t test). (*D*) Bar graphs indicate serum levels of leptin in MC4R$^{\Delta DAGL\alpha}$ (n = 13) and MC4R-Cre (n = 15) mice (unpaired t test). (*E* and *F*) The expression of certain genes normalized to *TBP* mRNA expression obtained by using qRT-PCR in eWAT and iWAT (unpaired t test). (*G–I*) Representative hematoxylin and eosin–stained sections of liver samples and the average fat vacuole sizes measured from liver sections from MC4R$^{\Delta DAGL\alpha}$ (n = 17) and MC4R-Cre (n = 14) mice. (*J*) The expression of certain relevant genes normalized to TBP mRNA expression obtained by using qRT-PCR from liver (unpaired t test). (*K* and *L*) Bar graphs indicate fasting blood glucose and serum insulin levels in MC4R$^{\Delta DAGL\alpha}$ (n = 16) mice and MC4R-Cre (n = 14) mice (unpaired t test). (*M*) Graphs indicate GTT in 50-wk-old male MC4R$^{\Delta DAGL\alpha}$ (n = 17) and MC4R-Cre (n = 14) mice after feeding on HFD ad libitum for 12 wk. Blood glucose levels were repetitively measured for 5 h following single ip injections of 2 gm/kg of body weight. (two-way ANOVA, Sidak's multiple-comparisons test). (*N*) The bar graphs indicate the AUC of blood glucose levels within the 4 h post glucose injections from experiment in *M* (unpaired t test). (*O*) Graphs indicate insulin tolerance testing performed in the same group of mice as in *M* showing blood glucose levels measured up to 3 h post ip injections of insulin 1 U/kg (two-way ANOVA, Sidak's multiple-comparisons test). (*P*) Bar graphs indicate the AUC of blood glucose levels within 3 h post insulin injections from experiments in *O* (unpaired t test). Data are presented as mean ± SEM. ns indicates $P > 0.05$, * indicates $P < 0.05$, ** indicates $P < 0.01$, *** indicates $P < 0.001$, and **** indicates $P < 0.0001$.

MC4R$^{\Delta DAGL\alpha}$ mice. We next tested the hypothesis that the MC4R$^{\Delta DAGL\alpha}$ mice are more glucose tolerant than Cre controls by conducting a glucose tolerance test (GTT). Blood glucose levels measured post glucose injection were significantly lower in MC4R$^{\Delta DAGL\alpha}$ mice than Cre mice (Fig. 3*M*). Furthermore, the area under the curve (AUC) of blood glucose indicates that MC4R$^{\Delta DAGL\alpha}$ mice had significantly lower blood glucose levels than that Cre mice (Fig. 3*N*), suggesting that MC4R$^{\Delta DAGL\alpha}$ mice are more glucose tolerant than Cre controls. We next tested the hypothesis that MC4R$^{\Delta DAGL\alpha}$ mice are more insulin sensitive than Cre controls by performing ip insulin tolerance test (ITT). We measured blood glucose levels up to 3 h post ip injection of insulin 1 U/kg. Blood glucose levels were significantly lower in MC4R$^{\Delta DAGL\alpha}$ mice than Cre control mice at multiple time points (Fig. 3*O*). Furthermore, the AUC of blood glucose levels was lower in MC4R$^{\Delta DAGL\alpha}$ mice than Cre animals (Fig. 3*P*), confirming the increased sensitivity of peripheral tissues to insulin.

Genetic Deletion of 2-AG Synthesis in MC4R Neurons Increases Energy Expenditure and Cardiovascular Function. Since defective 2-AG synthesis in MC4R neurons results in hypophagia, decreased body weight, and resistance to HFD, we hypothesized that energy expenditure could also be higher in MC4R$^{\Delta DAGL\alpha}$ mice compared to MC4R-Cre counterparts. We thus measured energy expenditure using indirect calorimetry by placing chow-fed mice in metabolic chambers at ambient temperatures. After two habituation days, two light and dark cycles were analyzed (Fig. 4*A*). The AUC from two dark and two light cycles indicates that energy expenditure is significantly higher in MC4R$^{\Delta DAGL\alpha}$ mice than MC4R-Cre controls during the dark cycle but not the light cycle (Fig. 4 *A* and *B*). We next conducted the analysis of covariance (ANCOVA) to compare values of energy expenditure normalized to the animals' lean body mass between MC4R-Cre and MC4R$^{\Delta DAGL\alpha}$ groups. Our analysis indicated that the slopes of energy expenditure were significantly different between MC4R-Cre and MC4R$^{\Delta DAGL\alpha}$ mice in the dark cycle but not light cycle (Fig. 4 *C* and *D*). The higher energy expenditure in MC4R$^{\Delta DAGL\alpha}$ mice is consistent with the prolonged suppression of weight gain observed after central DO34 infusion in wild-type mice (Fig. 1*I*) and could be, at least in part, due to increased thermogenesis.

In rodents, brown adipose tissue (BAT) is the main source of nonshivering thermogenesis. We investigated expression of BAT genes that regulate thermogenesis. Normalized gene expression values in BAT indicate significant increases in the expression of Prdm16, Elov13, cidea, cox7a1, and Mcad genes in MC4R$^{\Delta DAGL\alpha}$ mice compared Cre controls (Fig. 4*E*). Increases in *cidea*, *prdm16*, and *elovl3* expression suggest increases in thermogenesis machinery or "beiging" genes. Increases in *mcad* and *cox7* expression suggest increases in β-oxidation in BAT. Collectively, this profile is consistent with an increased BAT-mediated thermogenesis contributing to the increased energy expenditure observed in MC4R$^{\Delta DAGL\alpha}$ mice. In agreement with results of thermogenesis and BAT gene expression profile, BAT UCP1 protein was also found more abundant in MC4R$^{\Delta DAGL\alpha}$ mice compared Cre controls (Fig. 4 *F* and *G*).

Consistent with the MC4R-mediated increases in sympathetic output and energy expenditure, activation of MC4R increases mean arterial pressure (41), while antagonizing MC4R by icv administration of SHU9119 or AgRP reduces

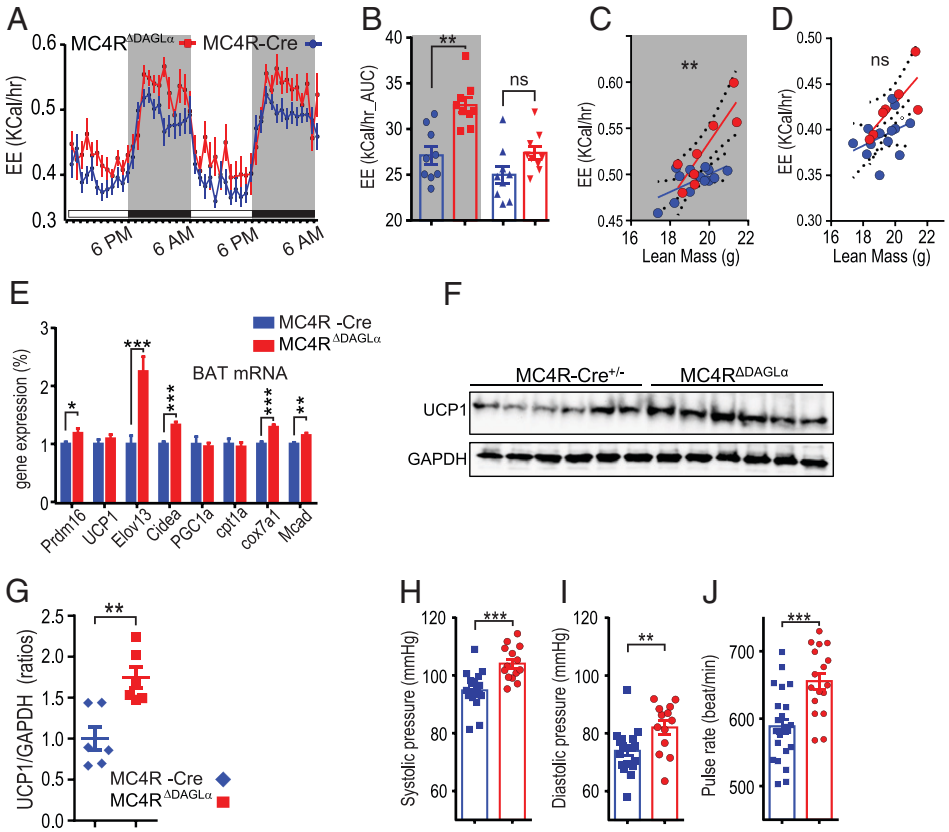

Fig. 4. Deletion of 2-AG synthesis from MC4R neurons results in increased energy expenditure, BAT-mediated thermogenic response and β-oxidation, and cardiovascular output. (*A*) Graphs indicate the energy expenditure of normal chow ad libitum–fed 30 wk-old male MC4R$^{\Delta DAGL\alpha}$ (n = 7) and MC4R-Cre mice (n = 7) during 2 d. (*B*) The graphs indicate the AUC of energy expenditure (kilocalories/hour) from two dark (gray shade) and two light cycles from *A* (one-way ANOVA, Tukey's multiple-comparisons test). (*C*) The analysis of covariance (ANCOVA) of energy expenditure normalized to animal's lean body mass (LBM) between MC4R-Cre and MC4R$^{\Delta DAGL\alpha}$ mice indicate the slopes of energy expenditure in MC4R-Cre (0.009 ± 0.004) and MC4R$^{\Delta DAGL\alpha}$ mice (0.03 ± 0.007) in the dark cycle (P = 0.008). (*D*) ANCOVA of energy expenditure indicate the slopes of energy expenditure from MC4R-Cre (0.0086 ± 0.006) and MC4R$^{\Delta DAGL\alpha}$ (0.021 ± 0.007) mice in the light cycle (P = 0.24). (*C* and *D* ANCOVA). (*E*) The expression of indicated thermogenic genes normalized to TBP mRNA expression obtained by using qRT-PCR from BAT (unpaired t test). (*F* and *G*) UCP1 and GAPDH protein expression in the BAT of the MC4R-Cre and MC4R$^{\Delta DAGL\alpha}$ mice analyzed by Western blot (*F*) and its quantification (*G*). (*H–J*) Bar graphs indicate the systolic (*H*) and diastolic (*I*) pressure and pulse rate (*J*) from 30-wk-old normal chow ad libitum–fed MC4R$^{\Delta DAGL\alpha}$ mice (n = 14) and MC4R-Cre mice (n = 18) measured using the noninvasive tail-cuff (unpaired t test). Data are presented as mean ± SEM. ns indicates $P > 0.05$, * indicates $P < 0.05$, ** indicates $P < 0.01$, *** indicates $P < 0.001$, and **** indicates $P < 0.0001$.

mean arterial pressure and heart rate (42). Furthermore, MC4R knockout mice and humans with MC4R heterozygous mutations are protected against hypertension despite increased body weight and hyperlipidemia (43). We thus hypothesized that cardiovascular function is dysregulated in MC4R$^{\Delta DAGL\alpha}$ mice. To test this hypothesis, we measured the systolic and diastolic pressure as well as pulse rate of these mice by using a noninvasive tail cuff. Results indicate that systolic and diastolic blood pressure as well as pulse rate are higher in MC4R$^{\Delta DAGL\alpha}$ mice than Cre controls (Fig. 4 *H–J*). Overall, this indicates increased cardiovascular activity in MC4R$^{\Delta DAGL\alpha}$ mice.

MC4R$^{\Delta DAGL\alpha}$ Mice Exhibit Elevated Basal Levels of Anxiety and a Thermogenic Response to Stress. A role of MC4R in mediating various aspects of stress has been shown in rodents (44). For example, injection of an MC4R agonist induces grooming in rodents (45). A role of eCBs mediating stress through various neuronal pathways has also been shown (46). We hypothesized that 2-AG released from MC4R neurons represents a signaling pathway that mediates anxiety-related behavioral responses. To test this, we compared the performance of MC4R$^{\Delta DAGL\alpha}$ and Cre mice in the Elevated Zero Maze (EZM), Open Field Test (OFT) and Tail Suspension Test (TST). Our data indicate that MC4R$^{\Delta DAGL\alpha}$ mice traveled a greater distance and spent more time in the closed arm and spent less time in the open arm and had less visits to the open arm in the EZM compared to Cre controls (Fig. 5 *A–D*). In the OFT, the MC4R$^{\Delta DAGL\alpha}$ mice traveled a greater distance and spent more time in the periphery than in the center. Within the periphery, they had greater distance to the center and traveled less in the center, traveled faster while in the center, and had higher freezing score compared to Cre controls (Fig. 5 *E–J*). Additionally, the MC4R$^{\Delta DAGL\alpha}$ mice were immobile for a longer duration in total than Cre mice in the TST (Fig. 5*O*). Collectively, these data suggest increased levels of anxiety in MC4R$^{\Delta DAGL\alpha}$ mice.

Genetic Deletion of 2-AG Synthesis from MC4R Neurons Increases Locomotion. MC4R mediates locomotive activity and MC4R null mice display decreased physical activity associated with hypometabolism compared to their weight-matched controls (47). We examined whether locomotion is different between MC4R$^{\Delta DAGL\alpha}$ mice and Cre controls. In the OFT, the MC4R$^{\Delta DAGL\alpha}$ mice traveled longer distance in total, had higher mean and maximal speed, and had more center-periphery crossings than Cre mice (Fig. 5 *K–N*). We also measured home cage locomotion using the Promethion system, which uses beam breaks in the three *x*-, *y*-, and *z*-axes. We observed that the MC4R$^{\Delta DAGL\alpha}$ mice displayed higher beam breaks in *x*- and *y*-axes in both light and dark cycles than Cre mice (Fig. 5*P*). Beam breaks in the *z*-axis were not significantly different (Fig. 5*Q*). Overall, these data suggest that genetic impairment of 2-AG synthesis in MC4R neurons enhances locomotor activity, consistent with the increase in energy expenditure described herein.

Since MC4R$^{\Delta DAGL\alpha}$ mice exhibited higher energy expenditure than Cre mice, we next examined whether stress could augment energy expenditure in MC4R$^{\Delta DAGL\alpha}$ mice. We used Promethion indirect calorimetry to measure the energy expenditure of MC4R$^{\Delta DAGL\alpha}$ and Cre control mice before and 3 d after a 30-min-per-day restraint stress (RS). We observed that 3 d of RS significantly increased energy expenditure in both the light and dark cycles in MC4R$^{\Delta DAGL\alpha}$ but not in Cre controls (Fig. 5 *R–T*). We also subjected mice to 30 min RS for 9 d from day 2 to 10 and monitored body weight and food intake for 47 d. We observed that RS induced hypophagia and weight loss

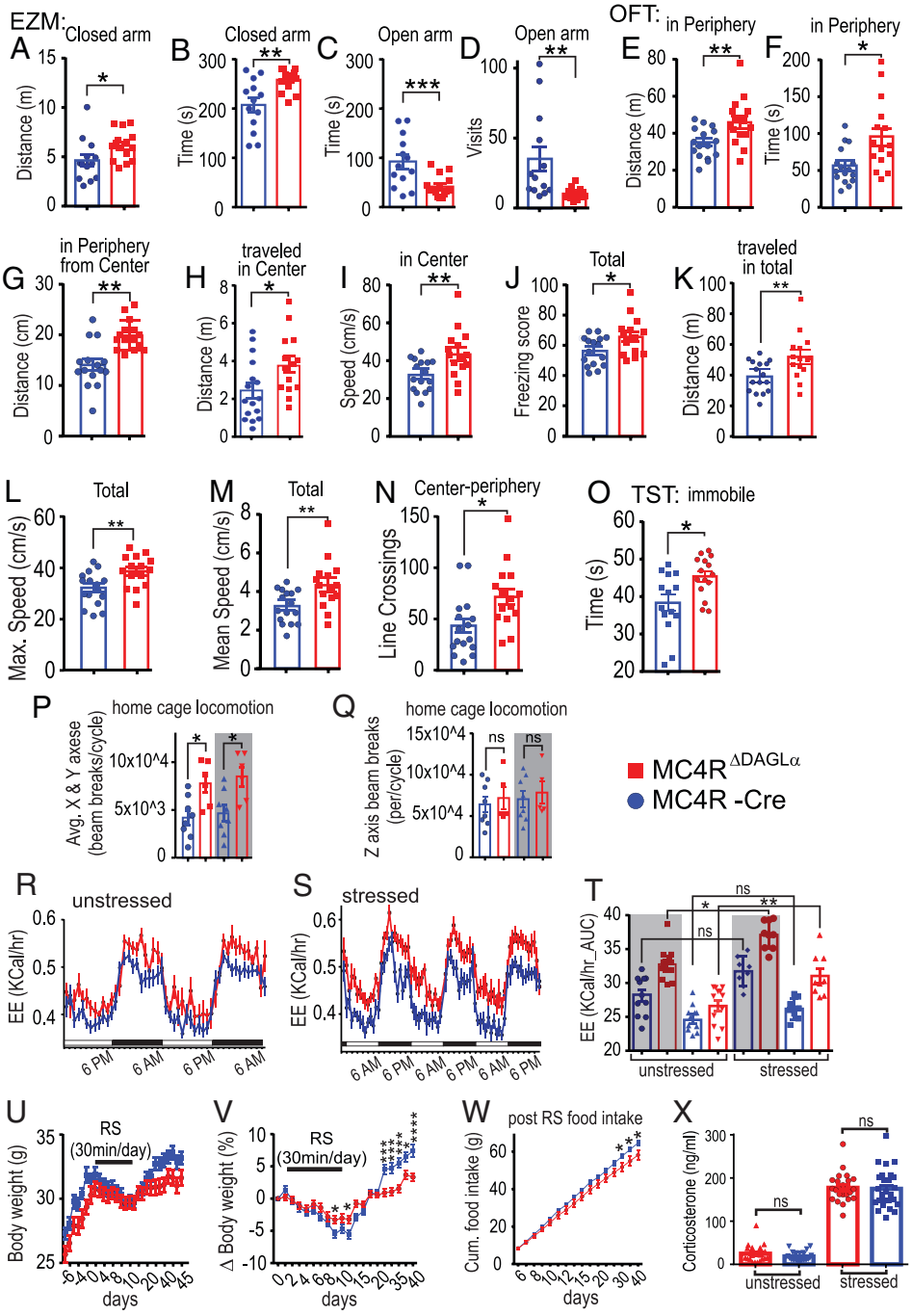

Fig. 5. Deletion of 2-AG synthesis from MC4R neurons results in elevated basal levels of anxiety and thermogenic response to stress. (*A–D*) The EZM results from MC4R$^{\Delta DAGL\alpha}$ (n = 15) and MC4R-Cre (n = 13) mice (unpaired t test). (*E–J*) The OFT results from MC4R$^{\Delta DAGL\alpha}$ (n = 15) and MC4R-Cre (n = 16) mice indicate anxiety behavior (unpaired t test). (*K–N*) The OFT results from MC4R$^{\Delta DAGL\alpha}$ (n = 15) and MC4R-Cre (n = 16) mice indicate the locomotion properties (unpaired t test). (*O*) TST results from MC4R$^{\Delta DAGL\alpha}$ (n = 15) and MC4R-Cre (n = 14) mice (unpaired t test). (*P* and *Q*) Home cage locomotion of MC4R$^{\Delta DAGL\alpha}$ (n = 8) and MC4R-Cre (n = 8) mice measured by using beam breaks in the x-, y-, and z-axes in the Promethion system. (*P*) The beam breaks in x- and y-axes averaged in both light and dark cycles (one-way ANOVA). (*Q*) The beam breaks in the z-axis between these groups of mice in the light and dark cycles (one-way ANOVA). (*R–T*) Energy expenditure (during two dark and two light cycles) of MC4R$^{\Delta DAGL\alpha}$ (n = 22) and Cre (n = 24) mice before (*R*) and after completion (*S*) of 3 d of RS for 30 min per day obtained by using Promethion indirect calorimetry. (*T*) The AUC obtained from *R* and *S* in MC4R$^{\Delta DAGL\alpha}$ and Cre mice (one-way ANOVA). (*U* and *V*) Effects of 30-min RS for 9 d on absolute (*U*), normalized (*V*) body weight, and the cumulative food intake (*W*) of MC4R$^{\Delta DAGL\alpha}$ (n = 22) and Cre (n = 24) mice (two-way ANOVA). (*W*) The cumulative food intake measured after RS from day 6 to day 40 which was significantly different from day 25 to 40 (multiple t test) in MC4R$^{\Delta DAGL\alpha}$ and Cre mice. (*X*) The serum corticosterone levels in the basal unstressed condition at 8 AM and 1 wk later after 10 min RS from MC4R$^{\Delta DAGL\alpha}$ (n = 23) and MC4R-Cre (n = 25) mice (unpaired t test). Data are presented mean ± SEM. ns indicates $P > 0.05$, * indicates $P < 0.05$, ** indicates $P < 0.01$, *** indicates $P < 0.001$, **** indicates $P < 0.0001$.

in both groups. The extent of weight lost was significantly less in MC4R$^{\Delta DAGL\alpha}$ mice than Cre controls (Fig. 5 *U* and *V*). Additionally, during recovery from RS, MC4R$^{\Delta DAGL\alpha}$ mice were unable to regain their original body weight as the Cre mice do. The normalized weight in MC4R$^{\Delta DAGL\alpha}$ mice remained significantly lower than Cre mice post RS (Fig. 5 *U* and *V*). The cumulative food intake measured after RS was significantly lower in MC4R$^{\Delta DAGL\alpha}$ mice than Cre mice (Fig. 5*W*).

Since stress activates the hypothalamic–pituitary–adrenal (HPA) axis and the MC4R$^{\Delta DAGL\alpha}$ mice exhibit heightened level of anxiety in baseline state and an increased thermogenic response to stress, we next examined whether stress would have differential effects on HPA axis activation in MC4R$^{\Delta DAGL\alpha}$ and Cre mice. We measured serum corticosterone levels at 8 AM, when the serum corticosterone levels are low in the basal unstressed condition, and again 30 min after a 10-min RS. MC4R$^{\Delta DAGL\alpha}$ and Cre mice did not differ in either basal or RS-induced serum corticosterone levels (Fig. 5*X*).

Discussion

Effects of cannabis and cannabinoids on stimulating appetite have long been known. Despite the centuries-long use of cannabinoids by humans, the cellular, synaptic, and circuit-level mechanisms by which eCBs regulate food intake and energy homeostasis are still incompletely understood (48). To fill this gap, we examined the effects of fasting on PVN^{MC4R} and specifically PVN^{MC4R}→LPBN neuron activity and their energy

state–dependent regulation by eCB signaling. Our study demonstrates that fasting increases AP firing of PVN^{MC4R} →LPBN neurons and increases tonic 2-AG-mediated inhibition of GABAergic transmission onto PVN^{MC4R} neurons. Levels of PVN 2-AG and tonicity of 2-AG-CB1R synaptic signaling are maximal during fasting and collapse in satiation, thus inversely correlating with energy state. Since the firing rate of PVN neurons is affected by GABAergic input from multiple nuclei including arcuate nucleus AgRP neurons, dorsomedial hypothalamus, and the bed nucleus of the stria terminalis, we propose that fasting-induced augmentation of tonic 2-AG signaling plays a critical role in the disinhibition of PVN^{MC4R} and specifically PVN^{MC4R} →LPBN neurons and facilitates initiation of feeding. If fasting-induced increases in 2-AG release stimulates food intake, disruption of this signaling should result in decreased food intake and body weight. Indeed, mice with impaired 2-AG synthesis within MC4R neurons are lean, hypophagic, and resistant to HFD-induced weight gain and metabolic syndrome. These observations are consistent with mid- to late-onset lean phenotypes observed in AgRP gene deletion, $AgRP^{GABA}$ neuron ablation (39, 40), and in DAGLα and CB1R knockout (KO) mice (49, 50). These data provide compelling evidence that 2-AG signaling at PVN^{MC4R} neuron afferent GABAergic synapses is an important mechanism regulating food intake and energy homeostasis.

Leptin functions as the main adipostatic factor in mammals and acts in part by modulating the AgRP–MC4R circuitry as an upstream signal (51). MC4R itself in our model is upstream of DAGLα signaling. Suppression of food intake by systemic blockade of 2-AG synthesis by ip injection of DO34 could occur through peripheral CB1R signaling. Also, the lean phenotypes observed in $MC4R^{\Delta DAGL\alpha}$ mice could be due to expression of MC4R in the periphery (36). Indeed, peripheral-to-central signaling pathways have been suggested to link endocannabinoids to the regulation of food intake and energy metabolism (52–54), and peripheral CB1R inverse agonism leads to leptin sensitization (34, 55). However, we show that central administration of DO34 suppresses food intake and weight gain. Furthermore, a subthreshold dose of icv DO34 was able to potentiate the anorectic effect of leptin, indicating that central 2-AG is sufficient to mediate the effects of systemic DO34 and that central 2-AG can also potentiate leptin signaling. Because MC4R is also expressed in the periphery, predominantly in the gut, we also tested the role of MC4R in the gut endothelium in energy balance by reconstituting MC4R expression in an otherwise MC4R null background. Gut-restricted MC4R re-expression did not affect the body weight or food intake of the animals compared to MC4R global knockouts. Combined with the other results in our study, we conclude that the phenotype observed in the $MC4R^{\Delta DAGL\alpha}$ mice is very likely due to its central effects. Because diet-induced obesity leads to hyperleptinemia and central leptin resistance, DAGLα inhibition stands as a promising weight loss approach in obesity, although its potential side effects on mood states will need to be evaluated. The leaner phenotype of the $MC4R^{\Delta DAGL\alpha}$ mice is in agreement with our finding that central inhibition of DAGL activity with DO34 potentiated leptin sensitivity. Thus, both peripheral and central components appear to mediate the physiological outcome of CB1R antagonism.

Our electrophysiological data suggest that 2-AG synthesized by PVN^{MC4R} neurons is a critical regulator of their activity. Deletion of DAGLα from all MC4R neurons ($MC4R^{\Delta DAGL\alpha}$ mice) or from all PVN neurons (injection of Cre-expressing virus into PVNs of adult $DAGL\alpha^{flox/flox}$) decreased food intake and body weight on standard diet and increased resistance to adiposity on HFD. These findings suggest that the hypophagia and DIO-resistance of $MC4R^{\Delta DAGL\alpha}$ mice are at least partially mediated via actions within PVN neurons. We cannot, however, exclude the possibility that $MC4R^{DAGL\alpha}$ deletion from neurons in nucleus accumbens also contributes to the absence of HFD-induced hyperphagia in $MC4R^{\Delta DAGL\alpha}$ mice (56).

The location of MC4R neurons that regulate energy expenditure is controversial, and recent studies suggest that distinct MC4R-expressing brain sites regulate food intake versus energy expenditure (13, 16, 57–59). Consistent with the phenotype of $MC4R^{\Delta DAGL\alpha}$ mice, deletion of CB1R from Sim1, CaMKIIα-, SF1 neurons, or the ventromedial nucleus of the hypothalamus increases energy expenditure (27, 60, 61). Despite these findings, it remains unclear whether 2-AG released from PVN^{MC4R} neurons mediates the increased energy expenditure in $MC4R^{\Delta DAGL\alpha}$. It is possible that 2-AG in PVN→NTS neurons mediate this effect. For example, activation of PVN^{CRH} neurons that project to the NTS increases energy expenditure (62). Alternatively, the sympathetic preganglionic IML neurons, which also express DAGLα, may be the site of action, as they express MC4R and their activation increases energy expenditure (57, 58, 63, 64). It is likely that DAGLα expressed in IML^{MC4R}→iBAT also regulates energy expenditure (16, 57, 58); however, this hypothesis remains to be tested.

Consistent with the findings from global CB1R and DAGLα knockout mice (49, 50), post-developmental deletion of PVN 2-AG signaling led to shortened life span in our study. Hypophagia and weight loss preceded death in PVN-Cre-$DAGL\alpha^{flox/flox}$ mice, but the cause of increased mortality is unclear. Disruption of both energy balance and cardiovascular function may increase the death rate in PVN-Cre-$DAGL\alpha^{flox/flox}$ mice. Consistent with the disrupted postfast refeeding response, administration of the selective MC4R agonist, LY2112688, failed to evoke an anorexigenic response in $MC4R^{\Delta DAGL\alpha}$ mice compared to control animals. Assuming intact MC4R signaling, a lack of response to LY2112688 in $MC4R^{\Delta DAGL\alpha}$ mice suggests that the ability of MC4R activation to suppress food intake is mediated via inhibition of 2-AG synthesis from MC4R PVN cells. Thus, we postulate that the MC4R neuron–specific ablation of 2-AG production results in a relatively high GABAergic tone and reduced AP firing of PVN^{MC4R} neurons and an occlusion of the effects of MC4R activation (65).

$MC4R^{\Delta DAGL\alpha}$ mice, like global CB1R and DAGLα knockout mice (49, 50), are lean and resistant to metabolic syndrome. We show here that this is in large part due to increased energy expenditure associated with increases in the BAT-mediated thermogenesis machinery and β-oxidation as well as increased physical activity. Analysis of the hypothalamus indicates significant increases in expression of AgRP and Orexin and decreased Kir7.1, suggesting a state of negative energy balance in the hypothalamic circuits of $MC4R^{\Delta DAGL\alpha}$ mice. Diet-induced obesity attenuates AgRP expression, likely as a consequence of hyperleptinemia; therefore, the increased AgRP expression we detected in the $MC4R^{\Delta DAGL\alpha}$ mice is consistent with their leaner phenotype. Additionally, WAT analysis indicates increased fatty acid synthesis, adipocyte "beiging," and increased lipogenesis suggesting an anabolic state, and liver analysis indicates improved liver function. In fact, increased activation of β-adrenergic signaling and β-oxidation has been shown to mediate the effects of chronic administration of rimonabant on induction of a negative energy balance (66). Furthermore, CB1R signaling in NTS sympathetic neurons has been documented, and transgenic mice lacking CB1R expression in these neurons display a lean phenotype, enhanced thermogenesis, and lipid oxidation (60). Thus, these findings suggest a profile of improved liver function, insulin sensitivity, reduced inflammation, and lower body weight under HFD feeding in $MC4R^{\Delta DAGL\alpha}$ mice compared to controls.

$MC4R^{\Delta DAGL\alpha}$ mice display elevated anxiety-like behavior. MC4R and CB1R signaling have been implicated in various aspects of anxiety (46, 67). Specifically, CB1R in Sim1-expressing neurons exerts tonic control on unconditioned anxiety, cued-fear expression, and locomotor reactivity, both with and without stress (68). We show here that $MC4R^{\Delta DAGL\alpha}$ mice exhibit increased anxiety-like and depressive-like behaviors, suggesting that 2-AG released from MC4R neurons serves an anxiolytic- and antidepressant-like function under physiological conditions.

We show here the functional interaction between two fundamental regulators of central energy homeostasis: the melanocortin and eCB systems. The intersection of these two pathways in hypothalamic feeding circuits could help elucidate therapeutic strategies to address a spectrum of metabolic diseases from anorexia to obesity. Pharmacological activation of MC4R signaling reduces food intake and promotes energy expenditure, cardiovascular activity, and lipid metabolism (17, 18). MC4R signaling has long been a target for development of therapeutic tools to treat obesity and eating disorders (20–22, 69). However, many attempts to activate MC4R signaling using orthosteric agonists have failed mainly due to unwanted, site-specific pressor effects (23). Our data suggest that the GABAergic input onto PVN^{MC4R} neurons is an important regulator of AP firing of these cells and that mechanisms regulating GABA transmission upstream of PVN^{MC4R} neurons could be targeted to indirectly regulate PVN^{MC4R} neurons and, thereby, energy homeostasis. Elucidating approaches to modulate PVN^{MC4R} neuron activity (e.g., through GABA inputs) could reveal opportunities for therapeutic intervention for metabolic disorders.

The effectiveness of such a potential tool is supported by the reduced efficacy of LY2112688 in $MC4R^{\Delta DAGL\alpha}$ mice, which are a model of presynaptic GABA-mediated dysregulation of PVN neurons. Thus, our work identifies DAGLα as a possible target for the treatment of obesity. CB1 receptor blockade (which prevents the cellular actions of both 2-AG and anandamide) has been previously shown to effectively reduce obesity in humans. Unfortunately, the CB1 receptor antagonist Rimonabant also elicited adverse neuropsychiatric effects, which led to its ultimate removal from clinical use (70). Specifically targeting 2-AG but not anandamide signaling may result in fewer adverse psychiatric effects while maintaining substantial metabolic efficacy; however, this remains to be further tested.

Experimental Procedure

Animal Models. All animal care and experimental procedures were approved by Vanderbilt University Medical Center Institutional Animal Care and Use Committee. Mice were maintained in a pathogen-free environment with ad libitum access to food and water, constant temperature, and humidity on a 12hr/12hr light/dark cycle unless otherwise specified. All mice were on a C57BL/6J background and the origin of each genetic strain is as indicated.

Hypothalamic Slice Electrophysiology. MC4R-GFP mice were deeply anesthetized with isoflurane and transcardially perfused with ice-cold and oxygenated cutting solution consisting of the following (in mM): 93 N-Methyl-D-glucamine, 2.5 KCL, 20 Hepes, 10 $MgSO_4{\cdot}7H20$, 1.2 NaH_2PO_4, 0.5 $CaCl2{\cdot}2H20$, 25 glucose, 3 Na^+-pyruvate, 5 Na^+-ascorbate, and 5 N-acetylcysteine. Slices were transferred to a holding chamber containing oxygenated artificial cerebrospinal fluid (aCSF; 24 °C) consisting of the following (in mM): 126 NaCl, 3.1 KCl, 1.2 $MgSO_4{\cdot}7H20$, 2.0 $CaCl2{\cdot}6H20$, 1 NaH_2PO_4, 26 NaHCO3, 10 glucose, 3 Na^+-pyruvate, and 1 Na^+-ascorbate. All drugs, except LY2112688, were stored in dimethyl sulfoxide (DMSO) stocks and then included in aCSF containing 1:2,000 (weight/volume) Bovine Serum Albumin (Thermo Fisher Scientific) and ≤ 1:2,000 (volume/volume) DMSO. Drugs were bath applied to the slice via the perfusion system (for extracellular applications) to perform recordings. LY2112688 was stored in saline stocks.

In this study, we examined effects of drugs on the AP firing as well as mIPSC frequency. The AP firing was recorded by using loosely sealed (1.8 to 2.2 MΩ), large extracellular pipettes filled with the aCSF in the extracellular mode (71). To record mIPSCs, MC4R-GFP neurons were voltage clamped and held around −70 mV in whole-cell configuration using borosilicate glass pipettes of 2 to 4 MΩ resistance when filled with internal solution containing the following (in mM): with 121 CsCl, 4 MgCl, 3 EGTA, 10 Hepes, 0.3 CaCl2, 4 NaATP, 0.3 NaGTP, 14 creatinine phosphate, pH ∼7.25 adjusted with CsOH, and osmolality of 295 to 300 mosmol/kg. Data were acquired at 10 kHz using a MultiClamp 700A amplifier (2,000× gain, −3-dB filter freq: 5 kHz) and Clampex 10.0.1 software (Axon Instruments, Union City). GraphPad Prism 6.0 (Graphpad Software, Inc., San Diego) and Excel 2010 (Microsoft, Bellevue) were used for data analysis. Statistical tests used included unpaired *t* test, repeated-measures (RM) one-way ANOVA, and RM two-way ANOVA as indicated.

LY2112688, α-MSH Analog, and DO34 Administration. The experimental groups were as follows: C57 wild-type (from Jackson Laboratory), $MC4R^{\Delta DAGL\alpha}$, and MC4R-Cre mice. All mice of each genotype were divided into two subgroups, and each subgroup was given either vehicle (equal volume) or 5 mg/kg LY2112688 (LY) in saline or 50 mg/kg DO34 in a 1:1:18 of ethanol: Kolliphor: saline solution at 10 mL/kg injections ip half an hour before beginning of the dark phase.

Chronic LY2112688 Infusions. For chronic LY infusions, Alzet osmotic pumps filled with LY were implanted in the subcutaneous space of the mice under isofluorene anesthesia. The body weight of the mice weas followed postsurgery for 2 wk.

Surgeries for Viral Injections. Mice were initially anesthetized with 5% isoflurane and then transferred to the stereotax (Kopf Instruments, Tujunga) and kept under 2% isoflurane anesthesia. For all surgeries, we used a motorized digital software (NeuroStar; Stoelting Co., Wood Dale) to guide a 10-μL microinjection syringe (Hamilton Co., Reno) driven by a Micropump Controller (World Precision Instruments, Sarasota). Virus (450 to 600 μL) was delivered bilaterally into the PVN [anteroposterior: −0.75, mediolateral (ML): ±0.35, and dorsoventral (lDV): 4.8] or LPBN (anteroposterior: −5.2, ML: ± 1.35, and DV: 3.50).

RS. Mice were brought into the restraint room and subjected to restraint in well-ventilated 50-mL tubes (plus 4-cm-long, easily removable middle tubes, which were slipped over the tail to restrict movement (between 9 and 11 AM) (72).

Behavior. All behavior was analyzed via ANY-maze (Stoelting, Wood Dale) software. All statistical tests are reported in the figure legends.

Viruses and Reagents. For deletion of DAGLα from PVN cells, AAV9-pENN-hSyn-HI-eGFP-Cre-WPRE-SV40 (Catalog no. 105540) (350 μL) was injected into bilateral PVNs. For electrophysiological interrogation of the LPBN-projecting PVN neurons, AAV2-CMV-RFP (Vector Biolabs) (250 μL) was injected into bilateral LPBNs of MC4R-GFP mice. SR141716 was obtained from NIDA Drug Supply Program, DO34 was obtained from Glixx Laboratories (Hopkinton), and JZL184 was obtained from Cayman Chemical (Ann Arbor). The

α-MSH analog, LY2112688, was obtained from Bachem (Bachem Laboratories).

Indirect Calorimetry. The Promethion SABLE system was used for indirect calorimetry. Mice were acclimated to the new cages for 3 d while fed ad libitum with normal chow. Mice were subjected to RS, as indicated. Food and water intake, locomotion, O_2 consumption, and CO_2 production were monitored continuously throughout the study.

GTT and ITT. The blood glucose levels were measured using a glucometer. The tail vein is pricked at its end with bleeding lancet or needle, and a small volume of blood is collected to the glucose strips placed in a glucose meter. To perform intraperitoneal (ip) GTT, mice were given single ip injections of 2 gm/kg of body weight glucose followed by repeated blood glucose measurements at minutes 20, 40, 60, 80, 100, 120, 140, 180, 210, 230, and 440 post injection. To conduct ip ITT. we measured blood glucose levels up to 3 h post ip injections of insulin 1 U/kg, at 15, 30, 45, 60, 75, 90, 120, 150, and 180 min.

Blood Pressure Measurement. The noninvasive mouse blood pressure measurement methodology (Kent Scientific) consists of utilizing a tail-cuff placed on the tail to occlude the blood flow. Upon deflation, noninvasive blood pressure sensors placed distal to the occlusion cuff can accurately and safely measure systolic and diastolic blood pressure as well as pulse rate in mice.

Body Composition. Whole-animal body composition analysis was performed by using the TD-NMR system Minispec Model mq7.5 (7.5 mHz; Bruker Instruments,) which is a benchtop-pulsed 7 T NMR system. The instrument gives lean-mass, fat-mass, and fluid-mass values.

Gene Expression Analysis Using q-PCR. Total RNA was isolated using TRIzol Reagent (Invitrogen) from frozen tissues. A total 1 μg of RNA was converted to complementary DNA (cDNA) (cDNA reverse transcription kit, Invitrogen) and used to screen expression levels of the listed genes. Reactions were amplified in an ABI Prism 7500 FAST sequence detector (Applied Biosystems) and acquired data were analyzed using the ΔΔCt method to determine the expression level of each transcript normalized to the expression level of the housekeeping gene, TATA box binding protein (TBP).

Corticosterone Measurements. Blood was collected from tail-vein pricks to obtain serum. If stressed, blood was collected in 20 to 30 min post RS. Enzyme-linked immunosorbent assay (ELISA) technique was used to measure corticosterone levels in the serum collected from mice by Corticosterone ELISA kit, Enzo Life Sciences, Inc, (ADI-900-097), as recommended by the manufacturer.

Liquid Chromatography with Tandem Mass Spectrometry Detection of Lipids. Mice underwent cervical dislocation immediately followed by decapitation. The brain was quickly removed, placed in a brain matrix, and covered with ice cold aCSF. One to two-mm–thick coronal sections containing the target brain regions were frozen on a metal block in dry ice. Dissections were performed on the frozen tissue to produce amygdala- and hypothalamus–enriched samples using a 1- or 2-mm diameter metal micropunch. Samples were stored at −80 °C until extraction. Liquid Chromatography with Tandem Mass Spectrometry detection of endocannabinoids and arachidonic acid was performed as previously described with minor modifications (73).

Fluorescent In Situ Hybridization for MCR4 and DAGLα mRNA. Various mRNA species expressed by PVN neurons were visualized with a variation of FISH using hybridized chain reaction version 3 method (Molecular Instruments). The probe sets directed against GAPDH, MCR4, and DAGLa mRNA were designed from sequence information from their respective mouse RefSeq mRNA IDs. The methodology was conducted as described previously (74).

IHC. Adult MC4R-GFP mice were perfused transcardially with cold 0.9% saline followed by cold fixative (4% paraformaldehyde in borate buffer, pH 9.5). The tissue sections were then incubated for 48 h with guinea pig anti-DAGLα (Mackie Laboratory, Indiana University; Bloomington), chicken anti-GFP (Aves Labs), and rabbit anti-cFos (Cell Signaling) primary antibodies. Following primary antibody incubation, sections were rinsed several times in 0.02 M potassium phosphate buffers and then incubated for 2 h at room temperature in the same blocking buffer containing secondary antibodies conjugated with the following Alexa-Fluor fluorochromes: goat anti-guinea pig 568, goat anti-chicken 488, and goat anti-rabbit 647 (Life Technologies) (75).

Data Availability. All study data are included in the article and/or *SI Appendix*. We will commit to share all the data and lines of mouse or any resources that this research may have generated and make them readily available to the research community.

ACKNOWLEDGMENTS. We thank Megan Altemus for excellent technical assistance with breeding and maintenance of mouse colonies used in this study. The indirect calorimetry study was performed by the Vanderbilt Mouse Metabolic Phenotyping Center (DK059637 and 1S10RR028101-01). This study was supported by the National Institute of Diabetes and Digestive and Kidney Diseases (NIDDK) Pilot & Feasibility grant (M.G.-L.), the Qatar National Research Foundation grant (NPRP9-351-3-075, M.G.-L. and I.C.), R01 MH107435 grant (S.P.), NIDDK DRTC Pilot & Feasibility grant (N.B.), and R01 DA043982 grant (K.M.).

1. K. M. Flegal, D. Kruszon-Moran, M. D. Carroll, C. D. Fryar, C. L. Ogden, Trends in obesity among adults in the United States, 2005 to 2014. *JAMA* **315**, 2284–2291 (2016).
2. A. R. Lucas, C. S. Crowson, W. M. O'Fallon, L. J. Melton, 3rd, The ups and downs of anorexia nervosa. *Int. J. Eat. Disord.* **26**, 397–405 (1999).
3. K. M. Flegal, M. D. Carroll, R. J. Kuczmarski, C. L. Johnson, Overweight and obesity in the United States: Prevalence and trends, 1960-1994. *Int. J. Obes. Relat. Metab. Disord.* **22**, 39–47 (1998).
4. M. M. Finucane *et al.*, National, regional, and global trends in body-mass index since 1980: Systematic analysis of health examination surveys and epidemiological studies with 960 country-years and 9·1 million participants. *Lancet* **377**, 557–567 (2011).
5. National-Heart-Lung-Blood-Institute, *Managing Overweight and Obesity in Adults: Systematic Evidence Review from the Obesity Expert Panel, 2013. US National Institute of Health and Human Service* (National Heart Lung Blood Institute, 2013).
6. K. M. Flegal, B. I. Graubard, D. F. Williamson, M. H. Gail, Excess deaths associated with underweight, overweight, and obesity. *JAMA* **293**, 1861–1867 (2005).
7. P. G. Kopelman, Obesity as a medical problem. *Nature* **404**, 635–643 (2000).
8. L. Cristino, L. Palomba, V. Di Marzo, New horizons on the role of cannabinoid CB1 receptors in palatable food intake, obesity and related dysmetabolism. *Int. J. Obes. Suppl.* **4** (suppl. 1), S26–S30 10.1038/ijosup.2014.8. (2014).
9 J. Tam *et al.*, Peripheral Cannabinoid-1 receptor inverse agonism reduces obesity by reversing leptin resistance. Cell *Metab.* **16**, 10.1016 (2012).
10. D. Huszar *et al.*, Targeted disruption of the melanocortin-4 receptor results in obesity in mice. *Cell* **88**, 131–141 (1997).
11. I. Gantz *et al.*, Molecular cloning of a novel melanocortin receptor. *J. Biol. Chem.* **268**, 8246–8250 (1993).
12. K. G. Mountjoy, M. T. Mortrud, M. J. Low, R. B. Simerly, R. D. Cone, Localization of the melanocortin-4 receptor (MC4-R) in neuroendocrine and autonomic control circuits in the brain. *Mol. Endocrinol.* **8**, 1298–1308 (1994).
13 N. Balthasar *et al.*, Divergence of melanocortin pathways in the control of food intake and energy expenditure. *Cell* **123**, 493–505 (2005).
14. J. N. Betley, Z. F. Cao, K. D. Ritola, S. M. Sternson, Parallel, redundant circuit organization for homeostatic control of feeding behavior. *Cell* **155**, 1337–1350 (2013).
15. D. Atasoy, J. N. Betley, H. H. Su, S. M. Sternson, Deconstruction of a neural circuit for hunger. *Nature* **488**, 172–177 10.1038/nature11270 (2012).

16. A. S. Garfield *et al.*, A neural basis for melanocortin-4 receptor-regulated appetite. *Nat. Neurosci.* **18**, 863–871 10.1038/nn.4011 (2015).
17. S. J. Li *et al.*, Melanocortin antagonists define two distinct pathways of cardiovascular control by alpha- and gamma-melanocyte-stimulating hormones. *J. Neurosci.* **16**, 5182–5188 (1996).
18. W. Fan, B. A. Boston, R. A. Kesterson, V. J. Hruby, R. D. Cone, Role of melanocortinergic neurons in feeding and the agouti obesity syndrome. *Nature* **385**, 165–168 (1997).
19. G. S. Yeo *et al.*, A frameshift mutation in MC4R associated with dominantly inherited human obesity. *Nat. Genet.* **20**, 111–112 (1998).
20. P. Weyermann *et al.*, Orally available selective melanocortin-4 receptor antagonists stimulate food intake and reduce cancer-induced cachexia in mice. *PLoS One* **4**, e4774 10.1371/journal.pone.0004774 (2009).
21. F. Yao, R. G. MacKenzie, Obesity drug update: The lost decade? *Pharmaceuticals* **3**, 3494–3521 (2010).
22. K. Y. Chen *et al.*, RM-493, a melanocortin-4 receptor (MC4R) agonist, increases resting energy expenditure in obese individuals. *J. Clin. Endocrinol. Metab.* **100**, 1639–1645 10.1210/jc.2014-4024 (2015).
23. M. H. Humphreys, Cardiovascular and renal actions of melanocyte-stimulating hormone peptides. *Curr. Opin. Nephrol. Hypertens.* **16**, 32–38 (2007).
24. M. A. Diana, A. Marty, Endocannabinoid-mediated short-term synaptic plasticity: Depolarization-induced suppression of inhibition (DSI) and depolarization-induced suppression of excitation (DSE). *Br. J. Pharmacol.* **142**, 9–19 10.1038/sj.bjp.0705726 (2004).
25. B. S. Basavarajappa, Critical enzymes involved in endocannabinoid metabolism. *Protein Pept. Lett.* **14**, 237–246 (2007).
26. K. A. Seely, P. L. Prather, L. P. James, J. H. Moran, Marijuana-based drugs: Innovative therapeutics or designer drugs of abuse? *Mol. Interv.* **11**, 36–51 10.1124/mi.11.1.6 (2011).
27. P. Cardinal *et al.*, Cannabinoid type 1 (CB1) receptors on Sim1-expressing neurons regulate energy expenditure in male mice. *Endocrinology* **156**, 411–418 (2015).
28. D. Wang *et al.*, Whole-brain mapping of the direct inputs and axonal projections of POMC and AgRP neurons. *Front. Neuroanat.* **9**, 40 (2015).
29 J. J. An *et al.*, TrkB-expressing paraventricular hypothalamic neurons suppress appetite through multiple neurocircuits. *Nat. Commun.* **11**, 020–15537 (2020).
30. F. Luo *et al.*, Whole-brain patterns of the presynaptic inputs and axonal projections of BDNF neurons in the paraventricular nucleus. *J. Genet. Genomics* **46**, 31–40 (2019).
31. C. Miralpeix *et al.*, Hypothalamic endocannabinoids inversely correlate with the development of diet-induced obesity in male and female mice. *J. Lipid Res.* **60**, 1260–1269 (2019).
32. R. J. Bluett *et al.*, Endocannabinoid signalling modulates susceptibility to traumatic stress exposure. *Nat. Commun.* **8**, 14782 (2017).
33. A. M. Cruz-Martínez *et al.*, CB1 receptors in the paraventricular nucleus of the hypothalamus modulate the release of 5-HT and GABA to stimulate food intake in rats. *Eur. Neuropsychopharmacol.* **28**, 1247–1259 (2018).
34 J. Tam *et al.*, Peripheral Cannabinoid-1 receptor inverse agonism reduces obesity by reversing leptin resistance. *Cell Metab.* **16**, 167–179 (2012).
35. I. Cakir *et al.*, Leptin receptor signaling in Sim1-expressing neurons regulates body temperature and adaptive thermogenesis. *Endocrinology* **160**, 863–879 (2019).
36. B. L. Panaro *et al.*, The melanocortin-4 receptor is expressed in enteroendocrine L cells and regulates the release of peptide YY and glucagon-like peptide 1 in vivo. *Cell Metab.* **20**, 1018–1029 (2014).
37. B. B. Madison *et al.*, Cis elements of the villin gene control expression in restricted domains of the vertical (crypt) and horizontal (duodenum, cecum) axes of the intestine. *J. Biol. Chem.* **277**, 33275–33283 (2002).
38. I. Gantz *et al.*, Molecular cloning, expression, and gene localization of a fourth melanocortin receptor. *J. Biol. Chem.* **268**, 15174–15179 (1993).
39. S. Qian *et al.*, Neither agouti-related protein nor neuropeptide Y is critically required for the regulation of energy homeostasis in mice. *Mol. Cell. Biol.* **22**, 5027–5035 (2002).
40. K. E. Wortley *et al.*, Agouti-related protein-deficient mice display an age-related lean phenotype. *Cell Metab.* **2**, 421–427 10.1016/j.cmet.2005.11.004 (2005).
41. J. J. Kuo, A. A. Silva, J. E. Hall, Hypothalamic melanocortin receptors and chronic regulation of arterial pressure and renal function. *Hypertension* **41**, 768–774 (2003).
42 A. A. da Silva, J. J. Kuo, J. E. Hall, Role of hypothalamic melanocortin 3/4-receptors in mediating chronic cardiovascular, renal, and metabolic actions of leptin. *Hypertension* **43**, 1312–1317 (2004).
43 J. R. Greenfield *et al.*, Modulation of blood pressure by central melanocortinergic pathways. *N. Engl. J. Med.* **360**, 44–52 (2009).
44. S. Chaki, S. Ogawa, Y. Toda, T. Funakoshi, S. Okuyama, Involvement of the melanocortin MC4 receptor in stress-related behavior in rodents. *Eur. J. Pharmacol.* **474**, 95–101 (2003).
45. J. D. Mul, B. M. Spruijt, J. H. Brakkee, R. A. H. Adan, Melanocortin MC(4) receptor-mediated feeding and grooming in rodents. *Eur. J. Pharmacol.* **719**, 192–201 (2013).
46. M. Morena, S. Patel, J. S. Bains, M. N. Hill, Neurobiological interactions between stress and the endocannabinoid system. *Neuropsychopharmacology* **41**, 80–102 10.1038/npp.2015.166 (2016).
47. L. Ste Marie, G. I. Miura, D. J. Marsh, K. Yagaloff, R. D. Palmiter, A metabolic defect promotes obesity in mice lacking melanocortin-4 receptors. *Proc. Natl. Acad. Sci. U.S.A.* **97**, 12339–12344 (2000).
48. E. L. Abel, Cannabis: Effects on hunger and thirst. *Behav. Biol.* **15**, 255–281 (1975).
49. D. R. Powell *et al.*, Diacylglycerol lipase α knockout mice demonstrate metabolic and behavioral phenotypes similar to those of cannabinoid receptor 1 knockout mice. *Front. Endocrinol. (Lausanne)* **6**, 86 (2015).
50. D. Cota *et al.*, The endogenous cannabinoid system affects energy balance via central orexigenic drive and peripheral lipogenesis. *J. Clin. Invest.* **112**, 423–431 (2003).
51. M. L. Andermann, B. B. Lowell, Toward a wiring diagram understanding of appetite control. *Neuron* **95**, 757–778 (2017).
52. N. V. DiPatrizio *et al.*, Fasting stimulates 2-AG biosynthesis in the small intestine: Role of cholinergic pathways. *Am. J. Physiol. Regul. Integr. Comp. Physiol.* **309**, R805–R813 (2015).
53. N. P. Bowles *et al.*, A peripheral endocannabinoid mechanism contributes to glucocorticoid-mediated metabolic syndrome. *Proc. Natl. Acad. Sci. U.S.A.* **112**, 285–290 (2015).
54. I. Ruiz de Azua *et al.*, Adipocyte cannabinoid receptor CB1 regulates energy homeostasis and alternatively activated macrophages. *J. Clin. Invest.* **127**, 4148–4162 (2017).
55. L. Gautron, C. E. Lee, S. Lee, J. K. Elmquist, Melanocortin-4 receptor expression in different classes of spinal and vagal primary afferent neurons in the mouse. *J. Comp. Neurol.* **520**, 3933–3948 (2012).
56 B. K. Lim, K. W. Huang, B. A. Grueter, P. E. Rothwell, R. C. Malenka, Anhedonia requires MC4R-mediated synaptic adaptations in nucleus accumbens. *Nature* **487**, 183–189 (2012).
57. J. W. Sohn *et al.*, Melanocortin 4 receptors reciprocally regulate sympathetic and parasympathetic preganglionic neurons. *Cell* **152**, 612–619 (2013).
58. E. D. Berglund *et al.*, Melanocortin 4 receptors in autonomic neurons regulate thermogenesis and glycemia. *Nat. Neurosci.* **17**, 911–913 (2014).
59. B. P. Shah *et al.*, MC4R-expressing glutamatergic neurons in the paraventricular hypothalamus regulate feeding and are synaptically connected to the parabrachial nucleus. *Proc. Natl. Acad. Sci. U.S.A.* **111**, 13193–13198 (2014).
60. C. Quarta *et al.*, CB(1) signaling in forebrain and sympathetic neurons is a key determinant of endocannabinoid actions on energy balance. *Cell Metab.* **11**, 273–285 (2010).
61. P. Cardinal *et al.*, Hypothalamic CB1 cannabinoid receptors regulate energy balance in mice. *Endocrinology* **153**, 4136–4143 (2012).
62. K. Arase, D. A. York, H. Shimizu, N. Shargill, G. A. Bray, Effects of corticotropin-releasing factor on food intake and brown adipose tissue thermogenesis in rats. *Am. J. Physiol.* **255**, E255–E259 (1988).
63. S. S. Hu, K. Mackie, Distribution of the endocannabinoid system in the central nervous system. *Handb. Exp. Pharmacol.* **231**, 59–93 (2015).
64. R. Nyilas *et al.*, Molecular architecture of endocannabinoid signaling at nociceptive synapses mediating analgesia. *Eur. J. Neurosci.* **29**, 1964–1978 (2009).
65. S. H. Oliet, D. V. Baimoukhametova, R. Piet, J. S. Bains, Retrograde regulation of GABA transmission by the tonic release of oxytocin and endocannabinoids governs postsynaptic firing. *J. Neurosci.* **27**, 1325–1333 (2007).
66. L. Bellocchio *et al.*, Activation of the sympathetic nervous system mediates hypophagic and anxiety-like effects of CB_1 receptor blockade. *Proc. Natl. Acad. Sci. U.S.A.* **110**, 4786–4791 (2013).
67. S. Chaki *et al.*, Anxiolytic-like and antidepressant-like activities of MCL0129 (1-[(S)-2-(4-fluorophenyl)-2-(4-isopropylpiperadin-1-yl)ethyl]-4-[4-(2-methoxynaphthalen-1-yl)butyl]piperazine), a novel and potent nonpeptide antagonist of the melanocortin-4 receptor. *J. Pharmacol. Exp. Ther.* **304**, 818–826 (2003).
68. S. Dubreucq *et al.*, Cannabinoid type 1 receptors located on single-minded 1-expressing neurons control emotional behaviors. *Neuroscience* **204**, 230–244 (2012).
69. Z.-C. Fan, Y.-X. Tao, Functional characterization and pharmacological rescue of melanocortin-4 receptor mutations identified from obese patients. *J. Cell. Mol. Med.* **13** (9B), 3268–3282 (2009).
70. L. F. Van Gaal, A. M. Rissanen, A. J. Scheen, O. Ziegler, S. Rössner; RIO-Europe Study Group, Effects of the cannabinoid-1 receptor blocker rimonabant on weight reduction and cardiovascular risk factors in overweight patients: 1-year experience from the RIO-Europe study. *Lancet* **365**, 1389–1397 (2005).
71. K. A. Takahashi, R. D. Cone, Fasting induces a large, leptin-dependent increase in the intrinsic action potential frequency of orexigenic arcuate nucleus neuropeptide Y/Agouti-related protein neurons. *Endocrinology* **146**, 1043–1047 (2005).
72. S. Patel, P. J. Kingsley, K. Mackie, L. J. Marnett, D. G. Winder, Repeated homotypic stress elevates 2-arachidonoylglycerol levels and enhances short-term endocannabinoid signaling at inhibitory synapses in basolateral amygdala. *Neuropsychopharmacology* **34**, 2699–2709 (2009).
73. B. C. Shonesy *et al.*, Genetic disruption of 2-arachidonoylglycerol synthesis reveals a key role for endocannabinoid signaling in anxiety modulation. *Cell Rep.* **9**, 1644–1653 (2014).
74. M. Ghamari-Langroudi *et al.*, G-protein-independent coupling of MC4R to Kir7.1 in hypothalamic neurons. *Nature* **520**, 94–98 (2015).
75. K. Bouyer, R. B. Simerly, Neonatal leptin exposure specifies innervation of presympathetic hypothalamic neurons and improves the metabolic status of leptin-deficient mice. *J. Neurosci.* **33**, 840–851 (2013).